

Supporting information

Ozone Modification as Efficient Strategy for Promoting the Photocatalytic Effect of TiO₂ for Air Purification

*Fan Zhang,^{a,b,c} Bin Hong,^b Weisheng Zhao,^{*a,b} Yue Yang,^c Jun Bao,^c Chen Gao^{*c} and Song
Sun^{*c,d}*

^a Fert Beijing Institute, BDBC, School of Microelectronics, Beihang University, Beijing, 100191, China

^b Hefei Innovation Research Institute, Beihang University, Beijing 100191, China.

^c National Synchrotron Radiation Laboratory, Collaborative Innovation Center of Chemistry for Energy Materials, University of Science & Technology of China, Hefei, Anhui, 230029, China.

^d School of Chemistry and Chemical Engineering, Anhui University, Heifei, Anhui, 230601, China

*Email: weisheng.zhao@buaa.edu.cn (W. Zhao)

*Email: cgao@ustc.edu.cn (C. Gao)

*Email: suns@ustc.edu.cn (S. Sun)

Photocatalytic activity and *in-situ* DRIFTS measurements

The experimental set up used for evaluating photocatalytic activities of the samples for the photocatalytic degradation of gaseous toluene is almost the same utilized in our previous study,¹ as shown in Fig. S1. The set up consists of three parts: a gas feed system, a photocatalytic reactor and an analytical system. The photocatalytic activity was tested using a 400 mL quartz photoreactor (Part I in Fig. S1). 0.1 g of the sample was used for photocatalysis reaction (the specific process is the same as described in ¹). The sample of ozone modified TiO₂ was obtained in advance in the O₃ atmosphere with a fixed flow rate of ca. 20 sccm by a ozone generator for 4 hours. Our previous experiments show that the photocatalytic activity enhances with treatment time, and reaches maximum and remains almost unchanged when the treatment time is over 4 hours. The light source employed for the photocatalytic reaction was a 300 W Xe-arc lamp (PLS-SXE300UV, Beijing Perfectlight Technology Co.,Ltd.) equipped with an IR-cutoff filter for eliminating the thermal effect. Before the photocatalytic reaction, the photocatalytic reactor was kept in the dark for 30 min to reach the adsorption/desorption equilibrium on the photocatalyst surface, thus eliminating the adsorption effect. The concentrations of toluene and product CO₂ in the photocatalytic reactor were analyzed by a gas chromatograph (GC1690, Hangzhou Kexiao Scientific Instruments Co. Ltd) equipped with a flame ionization detector (FID) and a chromatographic column (KX-112, Lanzhou Institute of Chemical Physics). The initial toluene concentration was 500 ppmv, and the relative humidity level was R.H. 80%. The degradation rate of toluene was calculated by the equation of $(1 - C/C_0) \times 100\%$, where C_0 is the initial toluene concentration and C is the toluene concentration at intervals. The mineralization rate of toluene was calculated by the equation of $(C''/7(C_0 - C')) \times 100\%$, where C' and C'' are the

concentrations of toluene and CO₂ at 60 minutes of photocatalytic degradation of toluene, respectively.

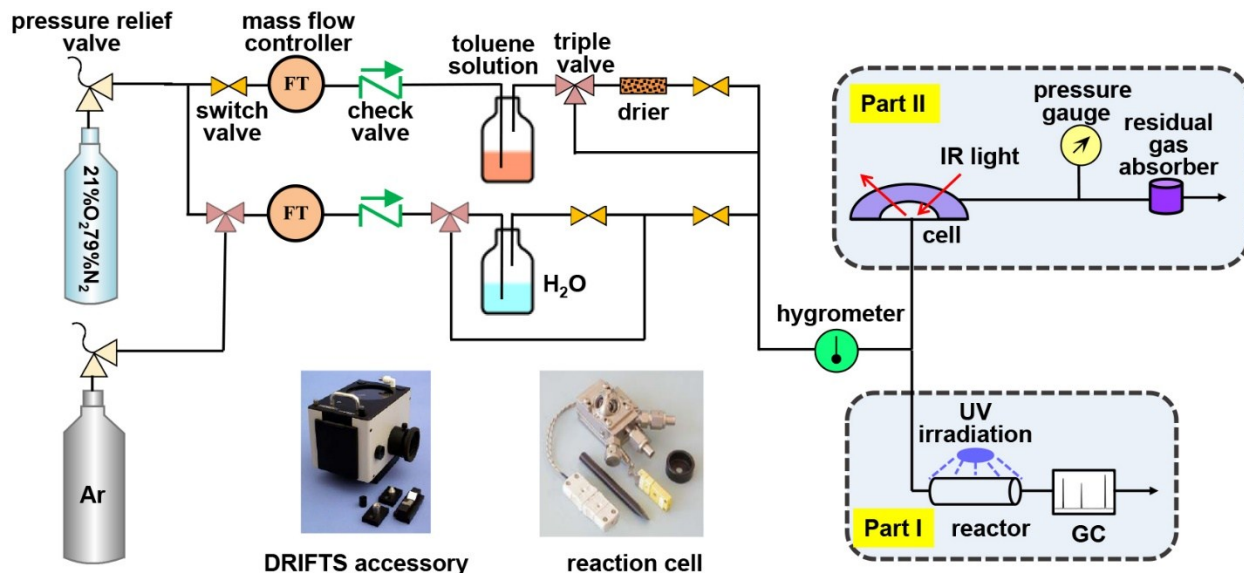


Fig. S1 Schematic diagram of the experimental setup for (Part I) the photocatalytic activity and (Part II) in situ DRIFTS measurements.

For in situ DRIFTS experiments, a Thermo Scientific Nicolet 8700 FTIR spectrometer at BL01B beamline of National Center for Protein Science Shanghai (NCPSS) at Shanghai Synchrotron Radiation Facility equipped with a liquid nitrogen cooled HgCdTe (MCT) detector was used and operated under OMNIC software. All the DRIFTS measurements were double-checked by using a Bruker IFS 66 v/s FTIR spectrometer at BL01B beamline of National Synchrotron Radiation Laboratory (NSRL) at University of Science and Technology of China (USTC). A reaction system (Part II in Fig. S1), consisting of a praying mantis DRIFTS accessory (Harrick Scientific) and a reaction cell (HVC, Harrick Scientific) was employed. The photocatalysts were housed in a sample cup inside the reaction cell. A dome with three windows covered the sample cup and was maintained in place with retaining plates. Two of the windows

were made of KBr and permitted entry and exit of the detection infrared beam, while the third was made of quartz to allow the photocatalyst to be irradiated by UV light. The details of the reaction system also can be found in.¹ The in situ DRIFTS spectra of toluene adsorption and photocatalytic degradation were collected in the range of 4000–600 cm^{-1} by averaging 64 scans with a resolution of 4 cm^{-1} .

Result of self-photolysis of gaseous toluene

Fig. S2 displays the degradation rate of toluene under irradiation without the photocatalyst with the initial concentration of 500 ppmv under R.H. 80%. Only about 2.9% of the toluene was self-photolyzed after 1 h irradiation.

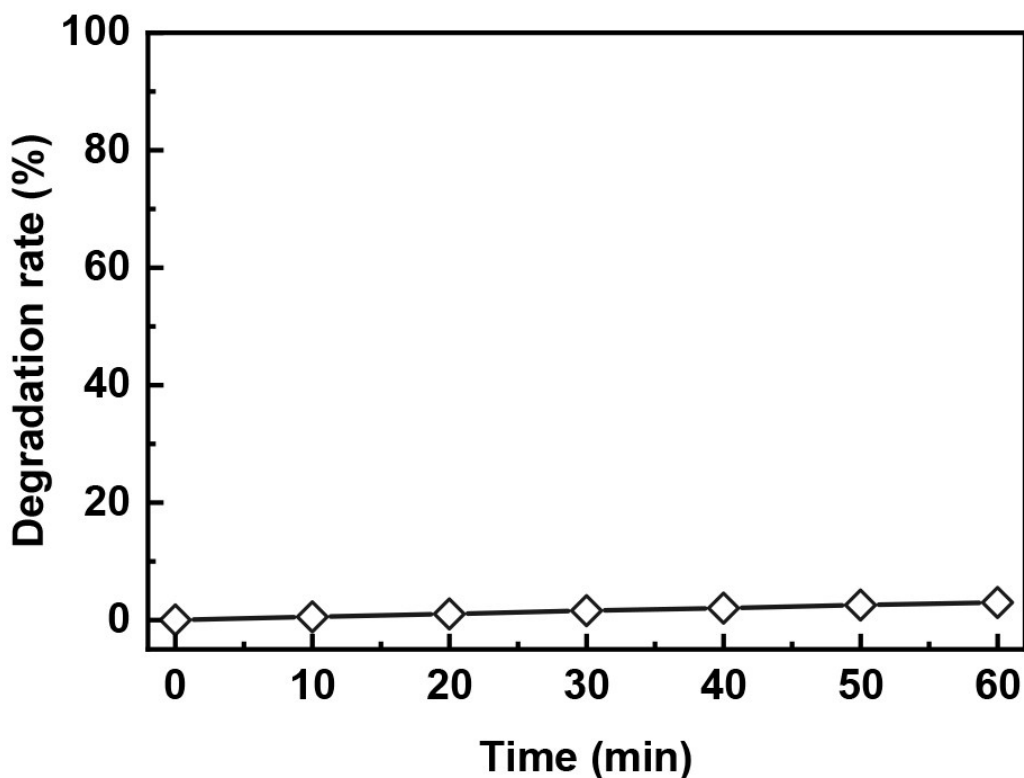


Fig. S2 Self-photolysis of gaseous toluene.

The spectrum of the light source used in the experiment

The light source used in this study did not contain UV light with wavelengths below 300 nm. The light with wavelengths at around 180 nm are considered to initiate ozone photolysis.²

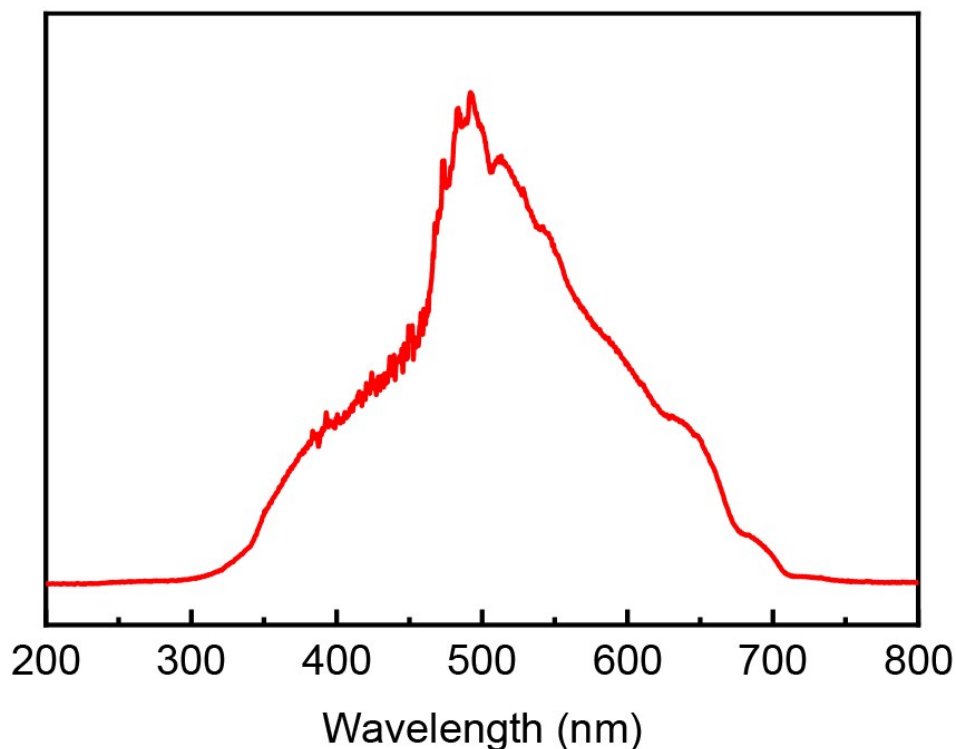


Fig. S3 The spectrum of the light source used in the experiment.

Detailed analysis of the differences between DRIFTS spectra of TiO_2 and $\text{O}_3\text{-TiO}_2$

The spectrum shown in Fig. S4 is obtained by subtracting the DRIFTS spectrum of TiO_2 from that of $\text{O}_3\text{-TiO}_2$. The bands at 3693 cm^{-1} and 3632 cm^{-1} are attributed to the stretching modes of different types of isolated hydroxyl groups.³ The broad band at 3215 cm^{-1} has been assigned to adsorbed water Ti-OH_2 species.⁴ The peak at 3663 cm^{-1} is assigned to OH groups situated on neighbouring titanium cations, whose proton is expected to be weakly bonded.⁵ Small bands in the $3900\text{-}3700\text{ cm}^{-1}$ range may be assigned to isolated hydroxyl groups.⁶ The band at 1634 cm^{-1}

is assigned to $\delta(\text{H}_2\text{O})$, and is shifted to 1627 cm^{-1} after ozone modification. According to the literature, the water molecules are first attached to the Ti5c sites on the surface of TiO_2 , and the other water molecules are then attached to the inner layer by H-bonds. And the H-bond structure blue-shift the bending vibration of H_2O , and the extent of this shift increases with the increase of the numbers of H-bonds.⁷ Therefore, the shift of the band at 1634 cm^{-1} reflect the decrease of the H-bonds. These results show that ozone modification causes the change of hydroxyl groups and water species on the surface of TiO_2 .

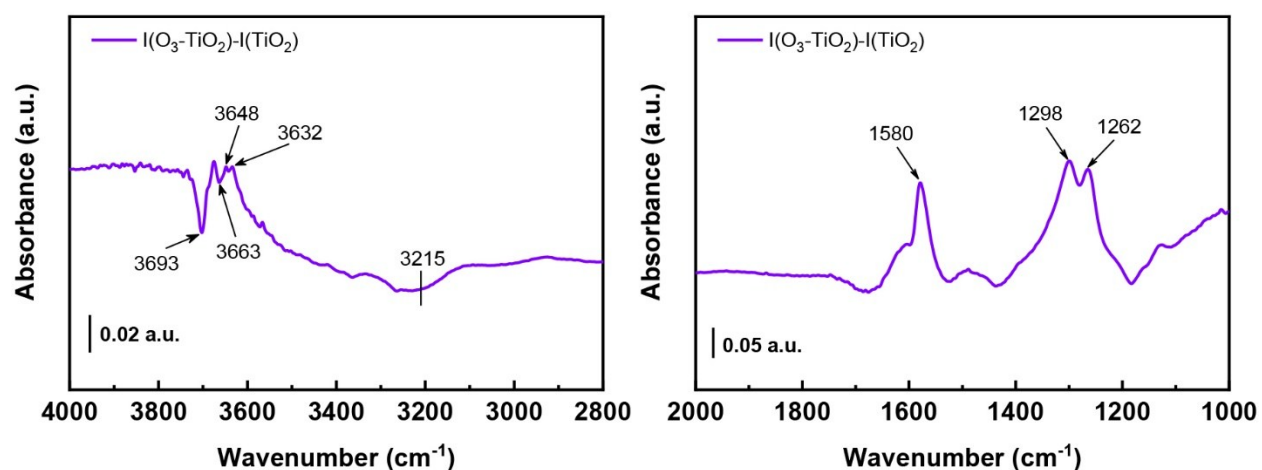


Fig. S4 The IR spectrum obtained by subtracting the DRIFTS spectrum of TiO_2 from that of O_3 - TiO_2 .

Computational methods

Herein, a molecular dynamics (MD) simulations were carried out in Materials Studio software developed by Accelrys using the Forcite module with the COMPASS force field. And this module yields accurate thermodynamic, kinetic, and structural results, providing an efficient adjunct to experiment. In addition, the methods provide insight into processes at the atomic level, allowing us to understand why and how a process occurs.

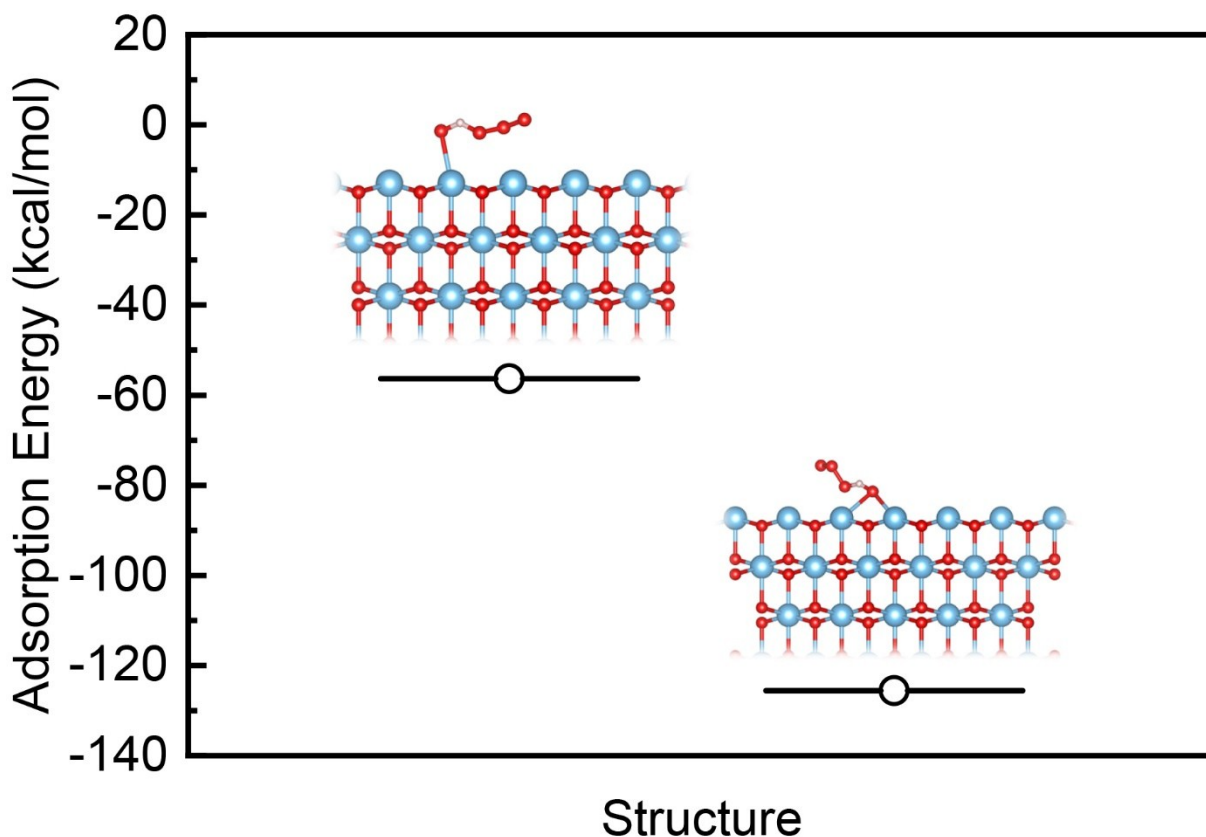


Fig. S5 Illustration of possible sites and adsorption energy for ozone molecule on terminal hydroxyl group and bridging hydroxyl group on (001) surface of anatase TiO₂.

The TiO₂ P25 used in this study contains about 80% anatase and 20% rutile. The anatase generally exhibits much higher photocatalytic activity for the photocatalytic degradation of volatile organic compounds than rutile. In this work we solely concentrate on the (001) surface of anatase TiO₂, which is the photocatalytic active surface in anatase.⁸ And the MD simulations elucidating the influence of the hydroxyl group site coupling with ozone molecules on (001) surface of anatase TiO₂ were calculated with employing the COMPASS force field (Fig. S5). The adsorption energy was calculated by using the following equation [Eq. (1)].

$$E_{\text{adsorption}} = E_{\text{total}} - (E_{\text{surface}} + E_{\text{ozone}}) \quad \text{Eq. (1)}$$

E_{total} is the total energy of ozone molecule adsorbed on surface bridging hydroxyl group or terminal hydroxyl group, E_{surface} is the energy of surface with bridging hydroxyl group or terminal hydroxyl group, E_{ozone} is the energy of ozone molecule.

The adsorption energy of ozone molecules on the bridging and terminal hydroxyl group is -125.6 and -56.4 kcal/mol (Fig. S5), respectively. This result shows that the ozone molecules adsorbed on the bridging hydroxyl group are more stable than that on the terminal hydroxyl group.

For further understanding the effect of ozone molecules on TiO_2 , the dissociation energy of water molecule on TiO_2 surface were calculated (Fig. 3). The dissociation energy was calculated by using the following equation [Eq. (2)].

$$E_{\text{dissociation}} = E_{\text{surface/OH+O}} - E_{\text{surface/H}_2\text{O}} \quad \text{Eq. (2)}$$

$E_{\text{surface/OH+O}}$ is the energy of adsorption of OH and H on the surface, $E_{\text{surface/H}_2\text{O}}$ is the energy of water molecule adsorbed on the surface.

The result shows that ozone modification facilitates the dissociative chemisorption of water molecules on the surface of TiO_2 .

XPS results

XPS was employed to characterize the chemical states of O and Ti atoms in the samples and the results are shown in Fig. S6 and Table S1. The peaks of binding energy located at 529.8 eV and 531.6 eV in the O 1s core level spectra were observed on the samples. The former peak was attributed to O^{2-} in the TiO_2 network, while the latter corresponded to oxygen in the surface hydroxyl groups. The proportion of O in the form of surface hydroxyl groups on $\text{O}_3\text{-TiO}_2$ is larger than that on TiO_2 . For the Ti 2p core level spectra, two peaks of binding energies located

at 458.6 eV and 464.3 eV were detected, corresponding to Ti 2p_{3/2} and Ti 2p_{1/2}, respectively, suggesting that Ti⁴⁺ is the main component in the two samples.

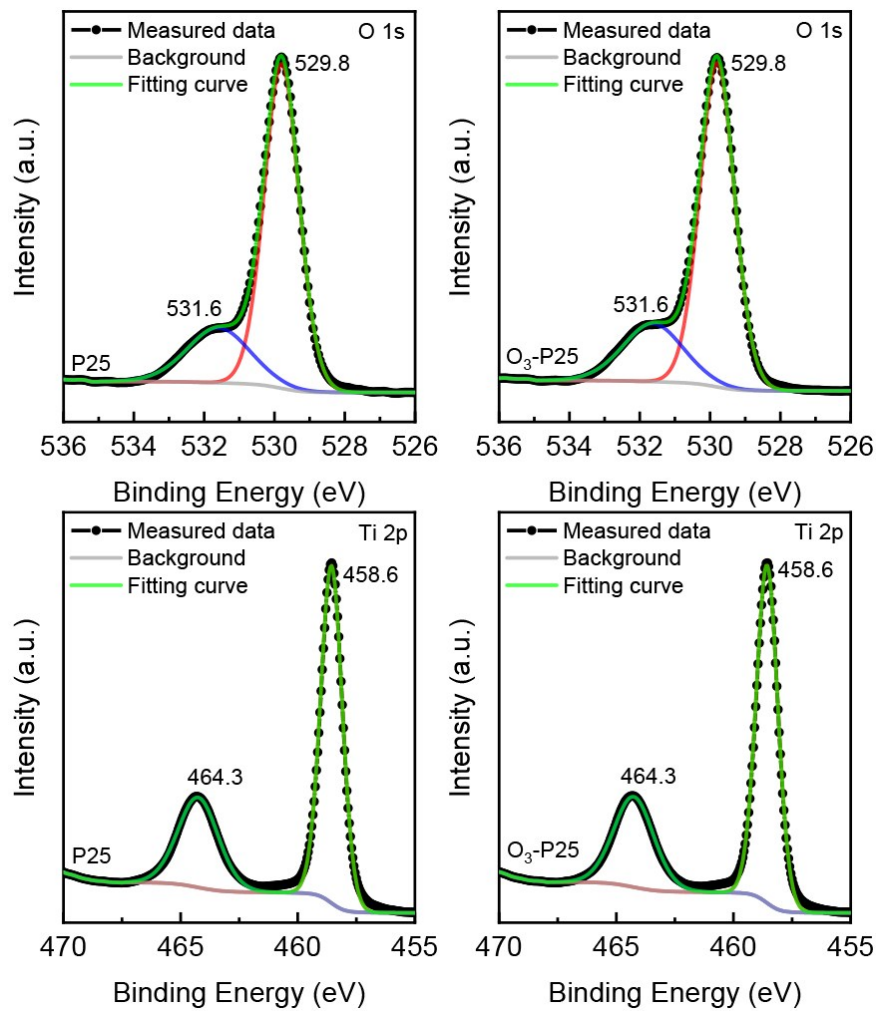


Fig. S6 XPS core level spectra of O 1s and Ti 2p for TiO₂ and O₃-TiO₂.

Table S1. XPS results

Sample	Element	Peak position	Peak Area	% Concentr.
P25	O1s(from TiO ₂)	529.79	209880.8	76.64
	O1s(from OH)	531.59	63966	23.36
	Ti 2p _{1/2}	458.55	89035.3	33.27
	Ti 2p _{3/2}	464.25	178551.4	66.73
O3-P25	O1s(from TiO ₂)	529.8	228488	75.37
	O1s(from OH)	531.62	74681.8	24.63
	Ti 2p _{1/2}	458.56	95842.5	33.14
	Ti 2p _{3/2}	464.25	193393.9	66.86

Vibrational frequency of ozone molecules based on QM/MM calculations on MD snapshot schemes.

To compare with experimental data obtained from the DRIFTS, the infrared spectra of O₃-TiO₂ were calculated in three situations: ozone modifies bridging hydroxyl group (Scheme a), Ti⁴⁺ ion (Scheme b) and water molecules (Scheme c) respectively using quantum mechanics/molecular mechanics (QM/MM) normal-mode vibrational frequency. And the dependence of the computed vibrational frequency of ozone on above mentioned three situations was investigated, and the results are presented in the Fig. S7. We note that the typically vibrational frequencies of ozone molecules are located at 1622 cm⁻¹ (Scheme a), 1589 cm⁻¹ (Scheme b) and 1605 cm⁻¹ (Scheme c), respectively. Moreover, the computed values are 1573, 1705 and 1597 cm⁻¹ for above mentioned three situations after the toluene molecule is introduced. Based on these results and DRIFTS, we speculate the characteristic band corresponding to the above three schemes of ozone on the surface of TiO₂.

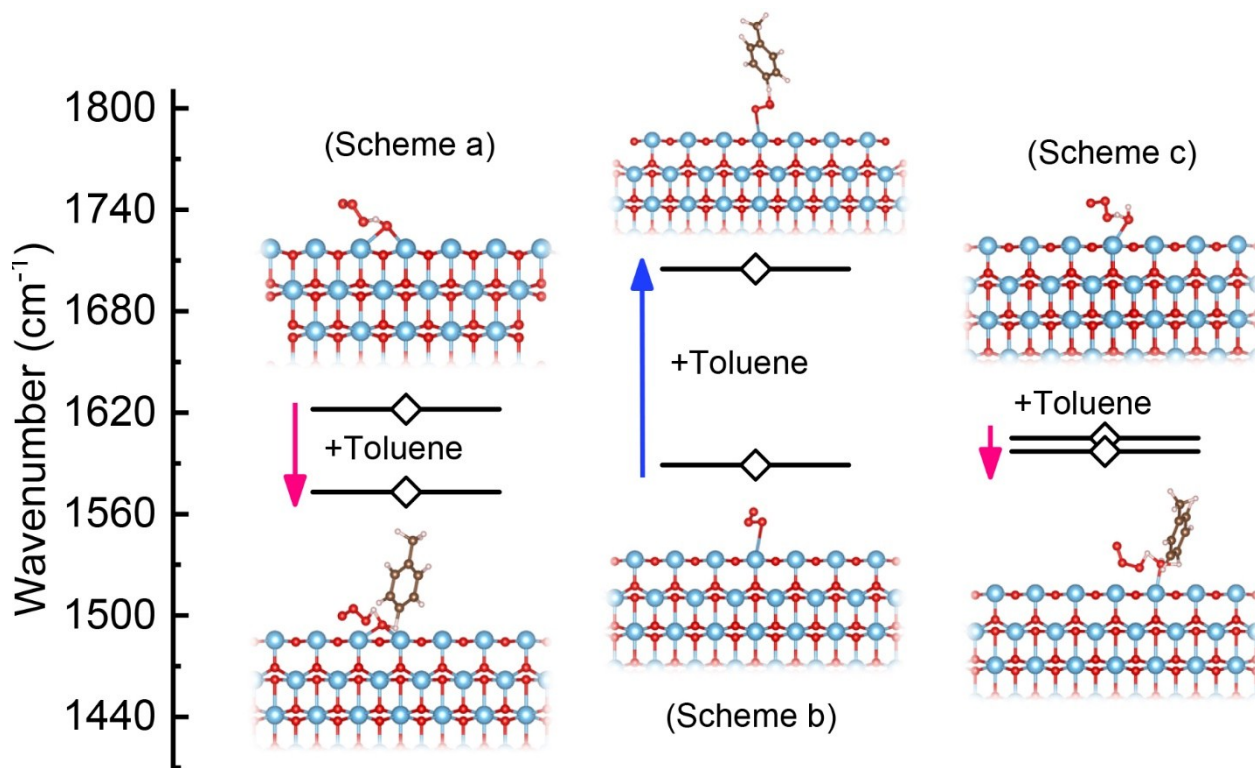


Fig. S7 Vibrational frequency of ozone molecules based on QM/MM calculations on MD snapshot schemes. (Scheme a) ozone interacts with bridging hydroxyl group, (Scheme b) ozone interacts with Ti^{4+} ion, (Scheme c) ozone interacts with water molecules.

Comparison of adsorption capacity of toluene on TiO_2 and $\text{O}_3\text{-TiO}_2$

The spectrum shown in Fig. S8 is obtained by subtracting the DRIFTS spectrum of 15 min in Fig. 4 (a) from that in Fig. 4 (b). The band at 3033 cm^{-1} is the characteristic band of toluene due to the $\nu_{\text{C-H}}$ of the aromatic ring. It is obvious that the area of this band on $\text{O}_3\text{-TiO}_2$ slightly larger than that on TiO_2 . This indicates that the adsorption capacity of toluene on $\text{O}_3\text{-TiO}_2$ is greater than that on TiO_2 .

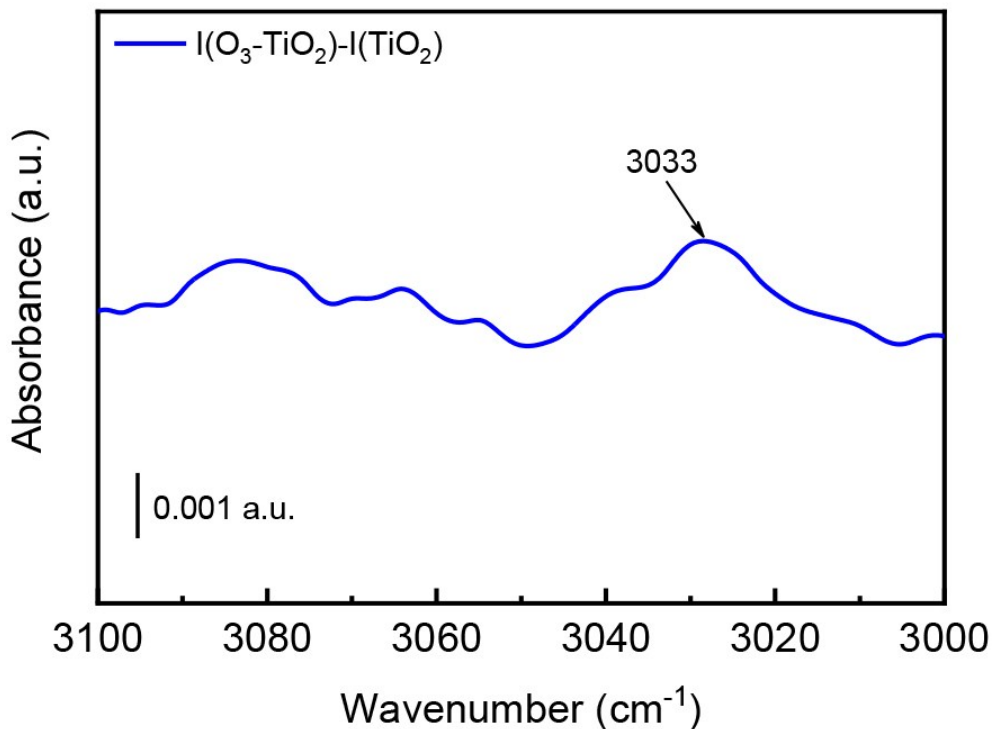


Fig. S8 Comparison of adsorption capacity of toluene on TiO_2 and $\text{O}_3\text{-TiO}_2$.

ESR results

To compare the amount of active radicals in the samples during the photocatalytic degradation, electron spin resonance (ESR) signals of the hydroxyl radicals and superoxide radicals spin trapped by 5,5-dimethyl-1-pyrroline-N-oxide (DMPO) in water and methanol, respectively, were recorded on a JES FA200 X-band spectrometer under irradiation with a 500 W Xe-arc lamp (Fig. S9). The characteristic signals in Fig. S9(a) indicated that $\text{O}_2^{\cdot-}$ radicals were generated during the photocatalytic reaction on $\text{O}_3\text{-TiO}_2$ and TiO_2 . The signal intensity showed that the amount of $\text{O}_2^{\cdot-}$ radicals generated on the $\text{O}_3\text{-TiO}_2$ is larger than that on TiO_2 . In Fig. S9(b), a characteristic 1:2:2:1 quartet signal was observed, which indicated that OH^{\cdot} radicals were generated during the photocatalytic reaction on the both samples. The amount of OH^{\cdot} radicals generated on the $\text{O}_3\text{-TiO}_2$ is approximately equal to that on TiO_2 .

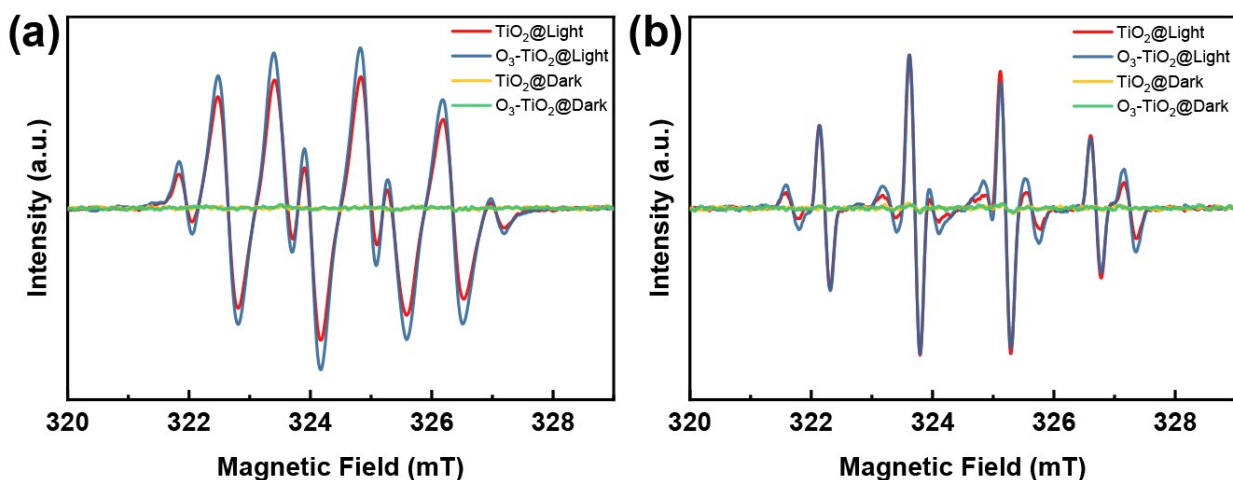


Fig. S9 DMPO spin-trapping ESR spectra for the (a) $\text{DMPO-O}_2^{\cdot-}$ and (b) DMPO-OH^{\cdot} of TiO_2 and $\text{O}_3\text{-TiO}_2$ with UV irradiation.

References

1. F. Zhang, M. Wang, X. Zhu, B. Hong, W. Wang, Z. Qi, W. Xie, J. Ding, J. Bao, S. Sun and C. Gao, *Appl. Catal., B*, 2015, **170-171**, 215-224.
2. J. Xiao, Y. Xie, F. Nawaz, S. Jin, F. Duan, M. Li and H. Cao, *Appl. Catal., B*, 2016, **181**, 420-428.
3. A. J. Maira, J. M. Coronado, V. Augugliaro, K. L. Yeung, J. C. Conesa and J. Soria, *J. Catal.*, 2001, **202**, 413-420.
4. P. A. Connor, K. D. Dobson and A. J. McQuillan, *Langmuir*, 1999, **15**, 2402-2408.
5. (a) M. D. Hernández-Alonso, S. García-Rodríguez, S. Suárez, R. Portela, B. Sánchez and J. M. Coronado, *Catal. Today.*, 2013, **206**, 32-39; (b) K. Hadjiivanov and D. G. Klissurski, *Chem. Soc. Rev.*, 1996, **25**, 61-39.
6. H. X. Lin, J. L. Long, Q. Gu, W. X. Zhang, R. S. Ruan, Z. H. Li and X. X. Wang, *Phys. Chem. Chem. Phys.*, 2012, **14**, 9468-9474.
7. H. Sheng, H. Zhang, W. Song, H. Ji, W. Ma, C. Chen and J. Zhao, *Angew. Chem. Int. Ed.*, 2015, **54**, 5905-5909.
8. H. G. Yang, C. H. Sun, S. Z. Qiao, J. Zou, G. Liu, S. C. Smith, H. M. Cheng and G. Q. Lu, *Nature*, 2008, **453**, 638-641.